Supporting Information

Regulation of π-π Interactions between Single Aromatic Molecules by Bias Voltage

Xiaona Xu[a], *Keqiang Jia*[a], *Qiang Qi*[b], *Guangjun Tian*[b*], *Xiang Dong*[a*]

[a] Center of Single-Molecule Sciences, Institute of Modern Optics, Tianjin Key Laboratory of Micro-scale Optical Information Science and Technology, Nankai University, Tianjin 300350, China.

[b] State Key Laboratory of Metastable Materials Science & Technology and Key Laboratory for Microstructural Material Physics of Hebei Province, School of Science, Yanshan University, Qinhuangdao, 066004, China.

Table of Contents

S.1 PSD of Three Types of Molecular Conductance

To gain a deeper understanding the origin of low conductance peaks, we analyzed the flicker noise of three molecules under both 0.1 V and 0.3 V conditions. Fig. S1 shows the noise power spectral density (PSD) spectra. We can find that the N value decreases as the bias voltage increases from 0.1 V to 0.3 V, indicating that the the π-π stacking is enhanced upon a higher bias voltage for all three types of molecules.

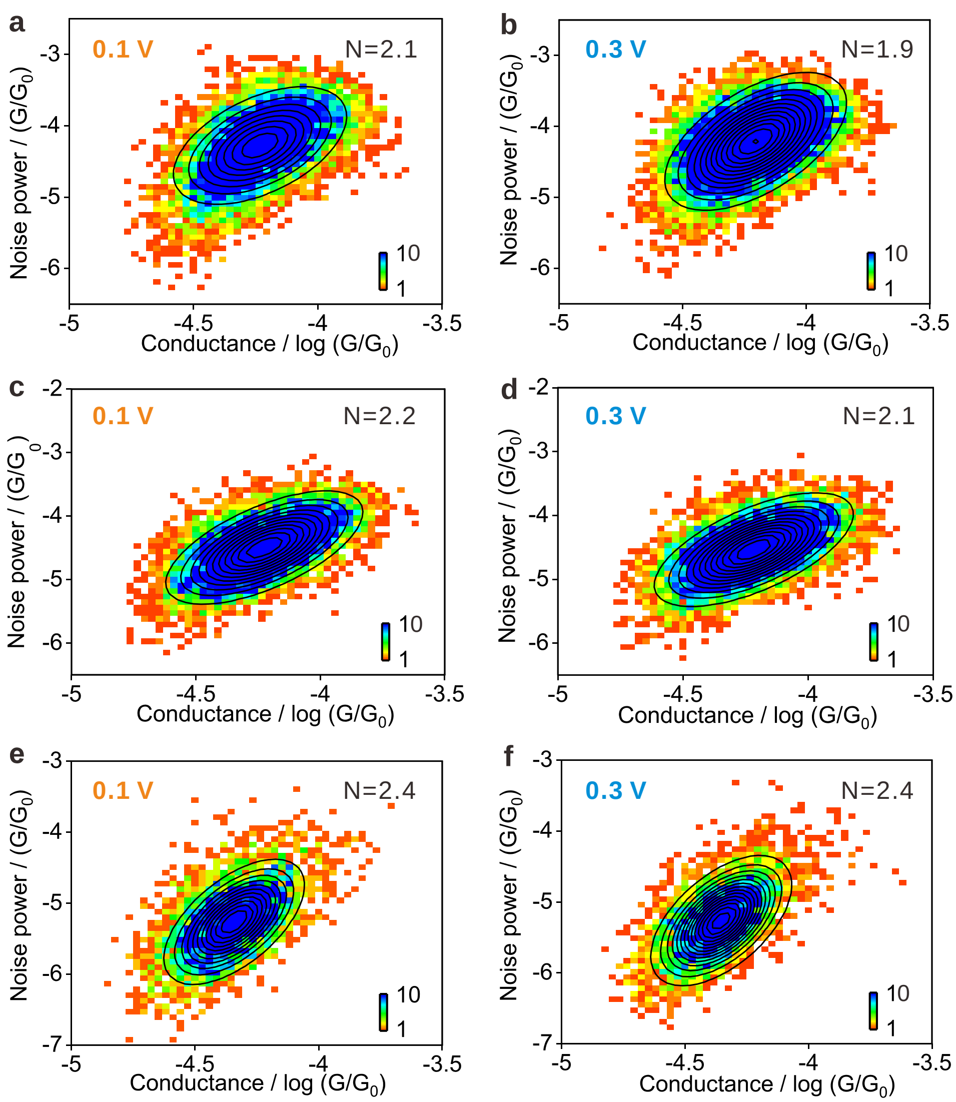

Figure S1. (a-f) The PSD spectra of β-NA, 2,6-NAP, and 5,6,7,8-THDA molecules at LC plateau state under 0.1 V and 0.3 V bias voltages, respectively.

S.2 2D Conductance Histograms of Molecular Conductance

In order to more intuitively display the characteristic peaks of molecular conductivity, we have listed the two-dimensional (2D) conductivity histograms of β-NA, 5,6,7,8-THDA, and 2,6-NAP three molecules under different bias voltages, as shown in Fig. S2a-f.

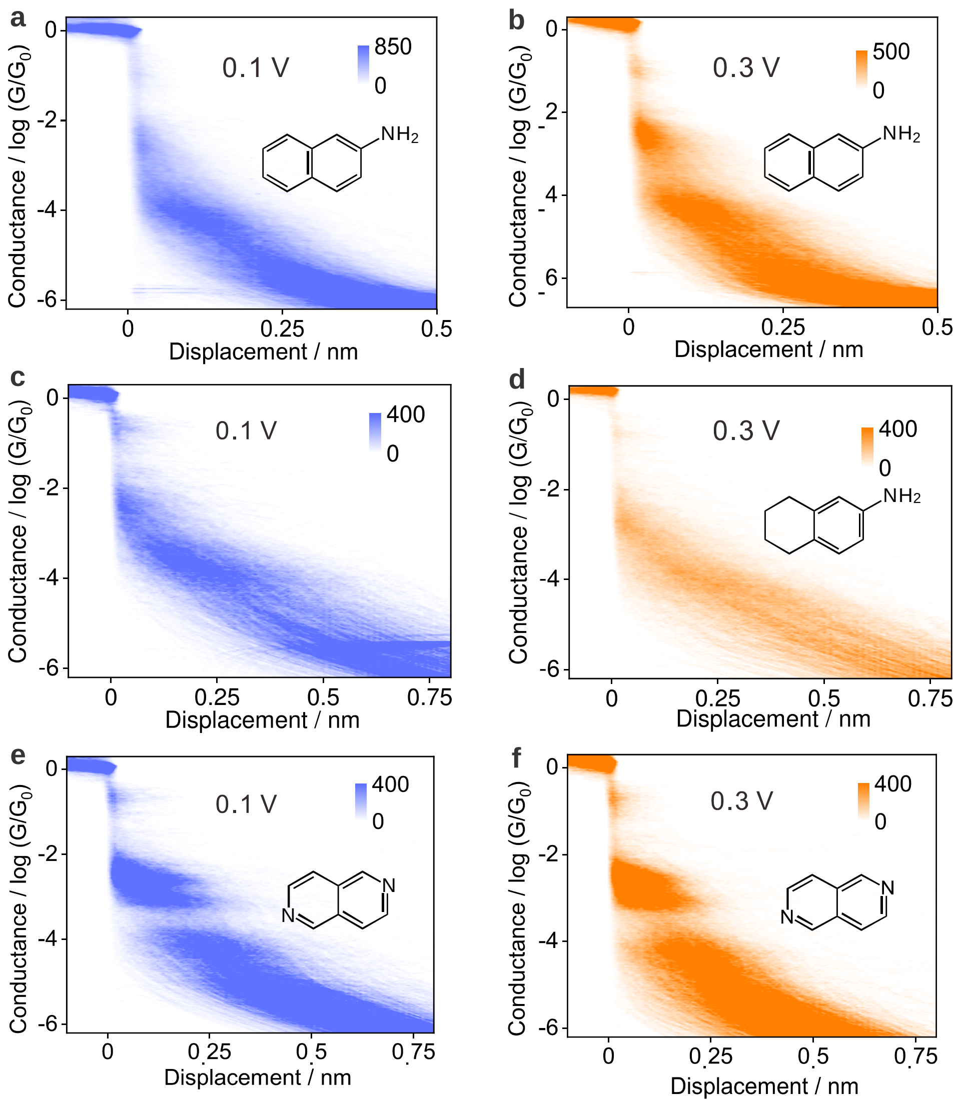

Figure S2. (a-f) Two-dimensional conductivity histograms of β-NA, 5,6,7,8-THDA and 2,6-NAP under different bias voltage. Insert: the schematic diagram of the molecules.

S.3 Excluding the Effect of Hydrogen Bond

Apart from the π-π stacking interactions occurring between benzene rings, amino-terminal molecules can also create dimers through hydrogen bonding between their amino groups. To verify the source of the LC peak in the molecular behavior, we introduced ethanol into the 1.2.4-Trichlorobenzene (referred to as TCB) solvent, thereby suppressing the formation of hydrogen bonds.[S1] Figure S3 shows that the LC peak can still be observed, and the intensity of the LC peak is enhanced upon higher bias. This observation confirms that the LC peak arises from the π-π stacking interactions between benzene rings, rather than the hydrogen bonding interactions. Furthermore, it can be found that the intensity of LC peak increases as the bias voltage increases from 0.1 V to 0.3 V, indicating the π-π coupling is enhanced when a higher bias voltage is applied on the molecular junctions.

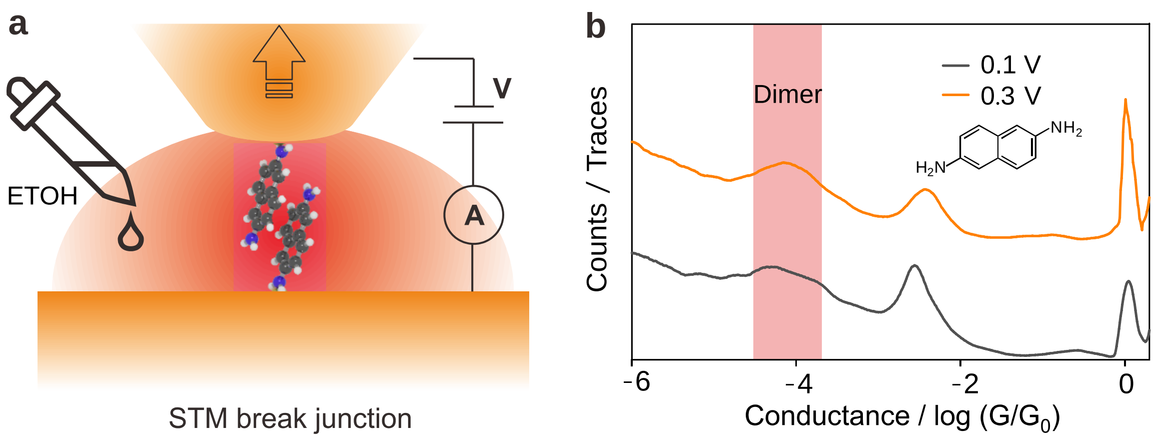

Figure S3. Excluding the possibility of hydrogen bonds. (a) Schematic of STM-BJ, adding ethanol into the TCB solvent (orange droplet). (b) 1D conductance histograms of 2,6-NDA molecules in TCB solvent with a small amount of ethanol under different bias voltages. The dashed area high light the LC peak, indicating the molecular dimer is formed *via* π-π intermolecular coupling rather than *via* hydrogen bonding.

S.4 Bias Voltage Dependent π-π Stacking

To investigate the modulation of the electric field on molecular π-π stacking, we performed bias-dependent experiments on four distinct molecular species in dark conditions, as shown in Fig. S4. The empirical findings reveal a discernible augmentation in the intensity of the low conductivity peak with the escalation of bias voltage, especially for 2,6-NDA, β-NA molecules. This finding substantiates the correlation between the enhancement of the low conductivity peak and the amplification of molecular dipole moment in response to the increased static electric field strength.

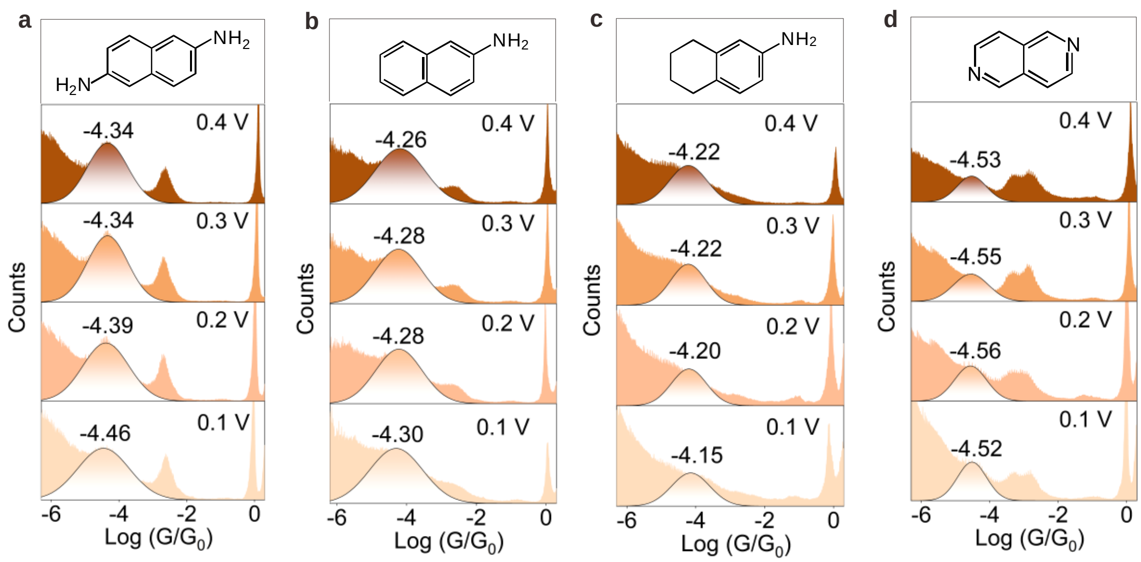

Figure S4. Conductance histograms depending on the bias voltage. (a-d) Shown the structures of 2,6-NDA, β-NA, 5,6,7,8-THDA, and 2,6-NAP four molecules, and the 1D conductance histogram of four molecules under different bias voltages.

S.5 Individual Conductance Traces

In order to demonstrate the effect of bias voltage more intuitively on the molecular structural dependent π-π stacking, we plot the conductance traces of four molecules. As shown in Figure S5, the length of the 2,6-NDA dimer conductance plateau increases. The enhancement of conductance steps for β-NA dimer is also evident, while this enhancement can not be easily recognized for 2,6-NAP and 5,6,7,8-THDA. These phenomena are consistent with the 1D and 2D conductivity histograms, as shown in the main text Figure 3.

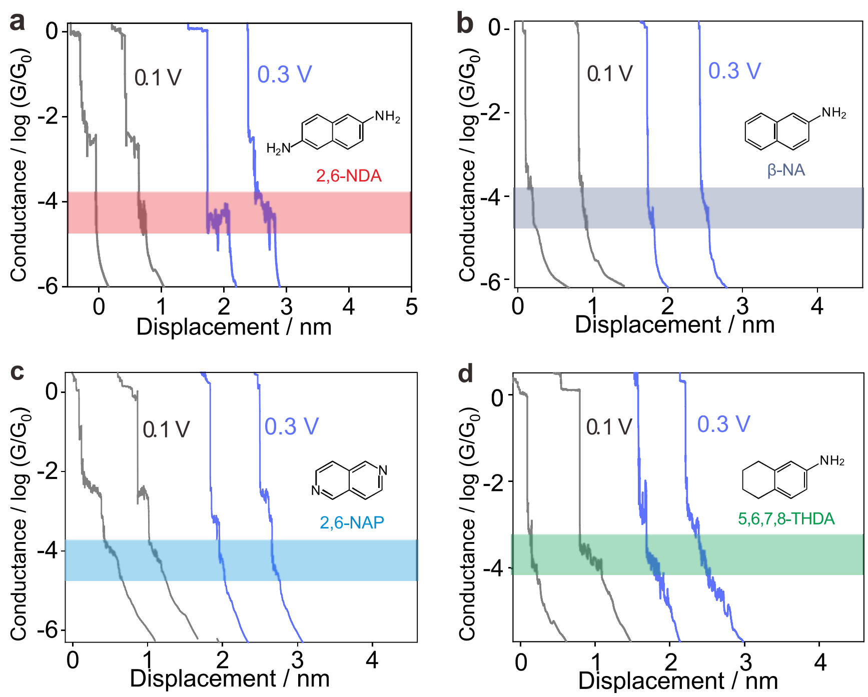

Figure S5. Individual conductance traces of all four molecules under bias voltages of 0.1 V and 0.3 V. Individual conductance traces of four kinds of molecules under low and high bias voltages. (a-d) Conductance trajectories of (a) 2,6-NDA, (b) β-NA, (c) 2,6-NAP, and (d) 5,6,7,8-THDA.

S.6 Transmission Spectrum of Molecular Dimers/Monomers

To ascertain the origins of the high and low conductance peaks, we conducted calculations of the transmission spectra with four respective molecular dimers/monomers junctions based on NEFG-DFT, as shown in Figs. S6 and S7. Detailed calculation process can be found in the method section. It can be found that the transmission coefficients of four dimers at Femi level are close and the transmission of molecular monomer junctions is approximately one order of magnitude larger than the one of molecular dimer junctions, which is in line with the experimental observation as present in Fig. 3 in the main text.

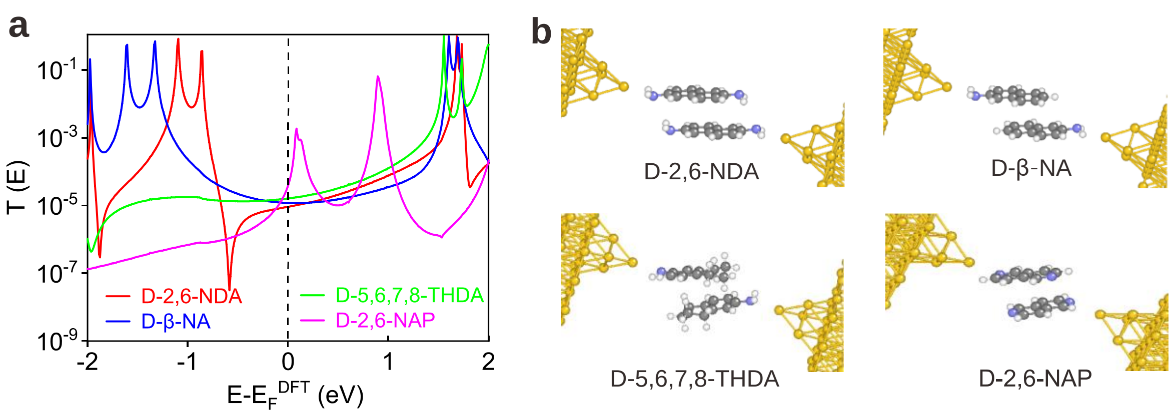

Figure S6. Theoretical calculations of transmission of four kinds of molecular dimer junctions. (a) Calculated transmission coefficient for four dimers. (b) Schematics of the dimer junctions for transmission calculations.

If we zoomed in on Figure S6a, we can find an anti-resonant peak located away from the Femi level, indicating a the destructive quantum interference. We attribute this anti-resonant peak of 2,6-NDA dimer to the intermolecular interaction between terminal amino groups, which is absent for β-NA (the sole amino group of β-NA is used to anchor the electrode already). In more detail, the QI effect can be understood from an orbital view.[2-4] In brief, t In brief, the flow of electrons through the two MO subunits is controlled by inter-orbital QI arising from the superposition of MOs. Destructive interference will occur when the $\Psi^H(\Upsilon_i)\Psi^H(\Upsilon_j)$ products from HOMO and $\Psi^L(\Upsilon_i)\Psi^L(\Upsilon_j)$ products from LUMO have the same signs. To reveal the underlying mechanism for the destructive quantum interference, we plot the frontier molecular orbitals of 2,6-NDA and β -NA dimer, as shown in Figure R2. For the 2,6-NDA dimer, the two connecting points exhibit the same color from the top view (same sign, designated as S) for both the HOMO and LUMO orbitals, thereby resulting in the DQI. In contrast, for β-NA dimer, the two connecting points have opposite colors for LUMO orbitals (designated as A), while they have the same colors for HOMO (designated as S), resulting in the absence of anti-resonant peak and the smooth transmission near the Fermi level.

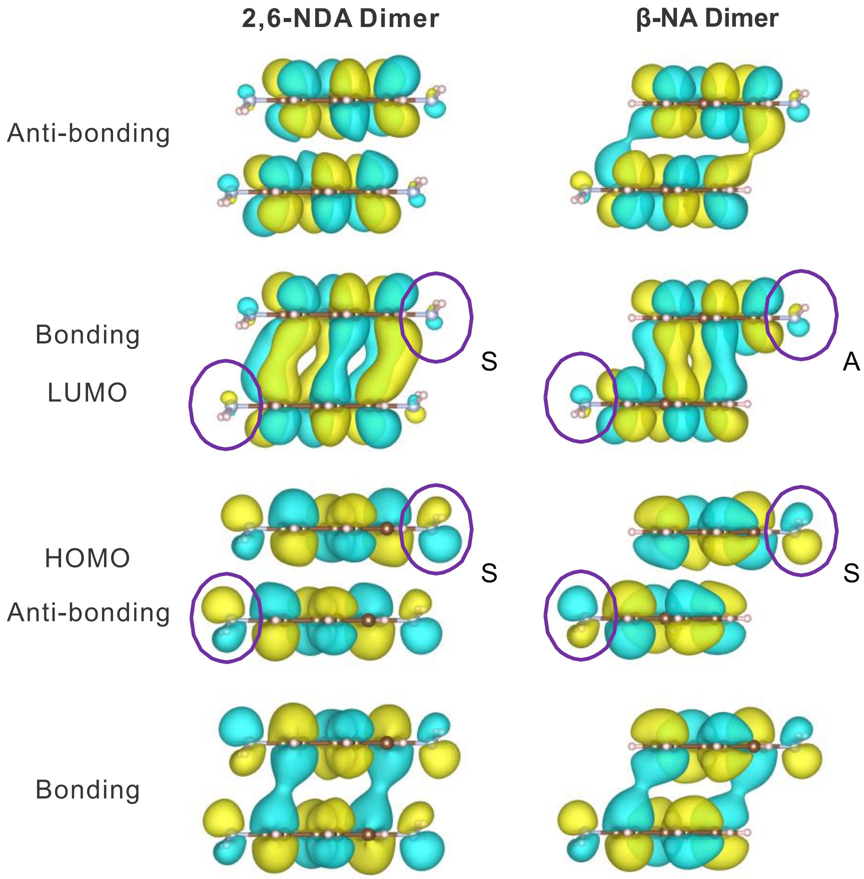

Figure S7. The dimerization of 2,6-NDA and β-NA induces the splitting of the HOMO and LUMO, forming bonding and antibonding pairs. For 2,6-NDA dimer, the injection and collection ends (marked by purple circles) exhibit the same color (marked as S) for both LUMO and HOMO. In contrast, two ends of β-NA dimer show opposite color (A) for LUMO, while they display the same color for HOMO.

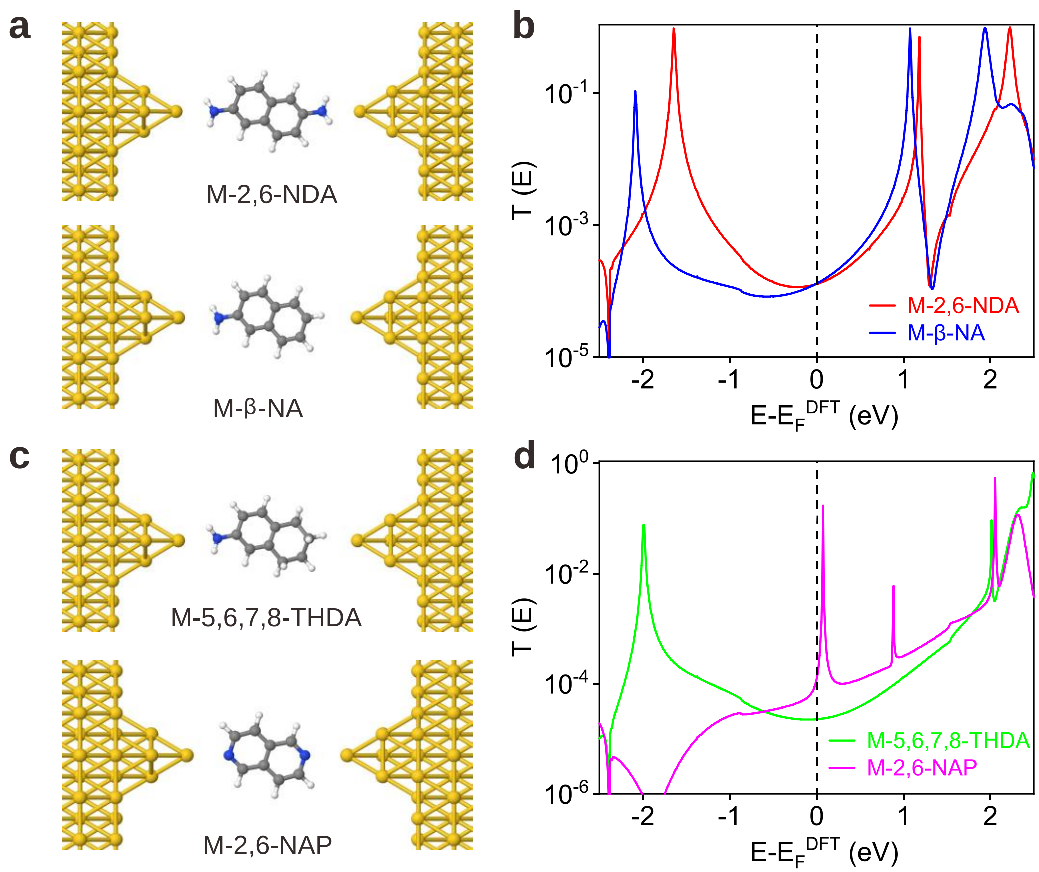

Figure S8. **Transmission functions of the four monomer molecular junctions.** (a) Schematic configurations of the molecular monomer junctions for 2,6-NDA and β-NA. (b) The transmission function of 2,6-NDA and β-NA monomer junctions. (c) Schematic configurations of the molecular monomer junctions for 5,6,7,8-THDA and 2,6-NAP. (d) The transmission function of 5,6,7,8-THDA and 2,6-NAP monomer junctions.

S.7 The Dipole Moments and Electrostatic Potential under Electric Field

Table S1. The dipole moments of four molecules are examined in the presence of electric fields of zero, 0.001 au, and 0.002 au. The last two columns in the data table indicate the discrepancies in dipole moments between the electric field strengths of 0.001 au. and zero, as well as between 0.002 au and 0.001 au, respectively.

Table S1. Dipole Moment of Molecular Monomers.

Dipole (Debye)	No field	0.001 au	0.002 au	Δ_{nof-1}	Δ_{1-2}
2,6-NDA	0	1.00	2.01	1.00	1.01
β-NA	2.58	3.25	3.98	0.67	0.73
5,6,7,8-THDA	1.70	2.03	2.48	0.33	0.45
2,6-NAP	0	0.44	0.89	0.44	0.45

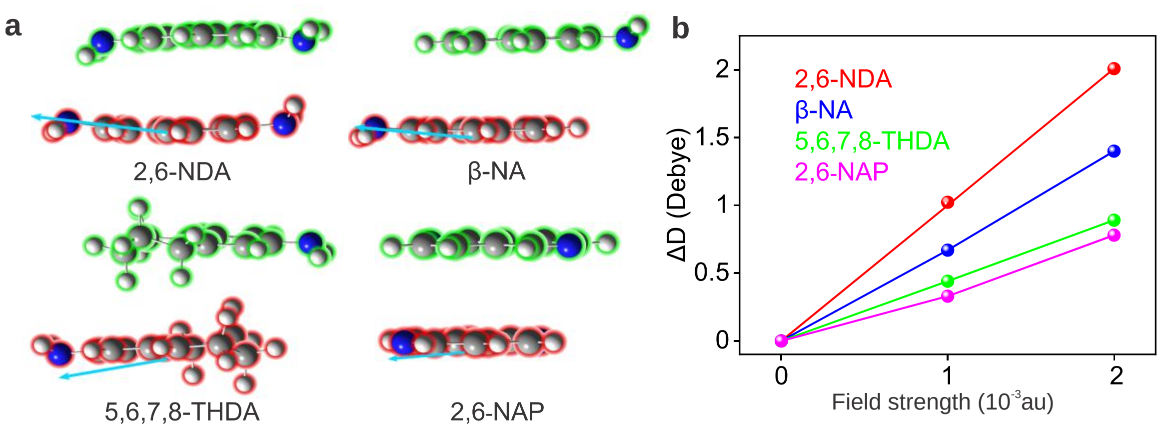

Figure S9. Dipole moment of the molecular dimers. (a) Schematic diagram of the dipole moment direction of four molecular dimers. (b) The change of the dipole moment values for four molecular dimers under different electric fields.

Table S2. Electron Electrostatic Potential.

By closely examining the ESP of 2,6-NDA and β-NA in Table S2, it is evident that the electric field significantly influences the ESP distribution around the amino groups (electron-donating group). The two amino groups at the ends of 2,6-NDA experience different field effects. When an electric field is applied along the X axis, i.e., parallel to the direction along the two nitrogen atoms, the negative ESP around the amino group on the left side weakens due to the attraction of the electric field. At the same time, the positive ESP remains relatively unaffected due to the combined influence of the right benzene ring and the electric field. In contrast, the ESP distribution around the right end of the amino group exhibits an opposite behavior: the positive potential weakens, and the negative electrostatic potential remains relatively unchanged. As a result, the overall ESP distribution of the molecule becomes asymmetric, generating a dipole moment along the direction of the external electric field.

Table S2. The electrostatic potential for the monomers of 2,6-NDA, β-NA, 5,6,7,8-THDA, and 2,6-NAP in zero and 0.002 au with different view perspectives.

Molecules	Field (au)	View direction		
		yx	-yx	zx
2,6-NDA	0.000	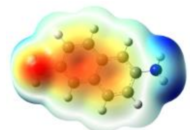	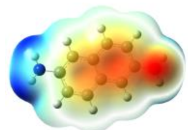	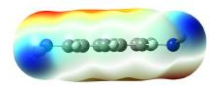
	0.002	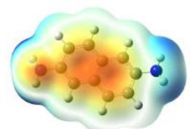	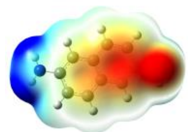	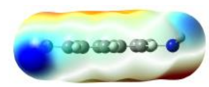
β-NA	0.000	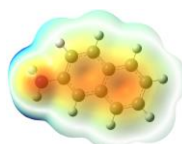	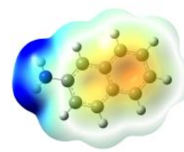	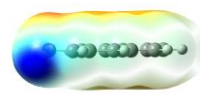
	0.002	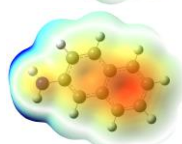	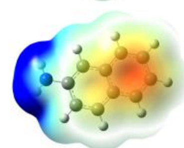	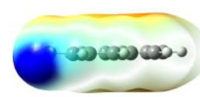
5,6,7,8-THDA	0.000	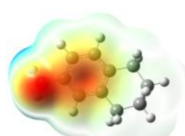	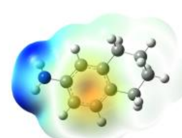	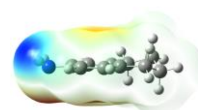
	0.002	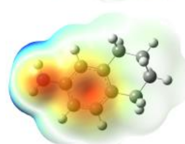	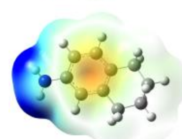	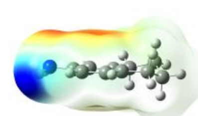
2,6-NAP	0.000	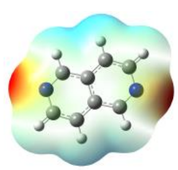	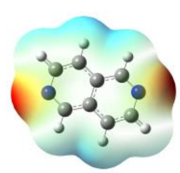	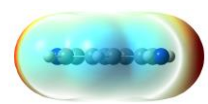
	0.002	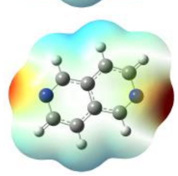	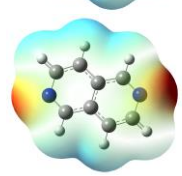	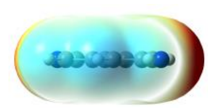

Table S3. Optimized Molecular Length.

Molecule	Monomer (Å)	Dimer (Å)
2,6-NDA	7.870	9.804
β-NA	6.450	9.751
5,6,7,8-THDA	6.529	8.700
2,6-NAP	5.044	7.173

S.8 Natural bond orbital (NBO) analysis of the 2,6-NDA monomer/dimer

We first computed the NBO of the 2,6-NDA monomer, as shown in Figure S10a and Table S4. From the results of the second-order perturbation energies, it is evident that in the absence of an electric field, the lone pair (LP) electron orbitals on the nitrogen exhibit the strongest interaction with the adjacent C-C antibonding orbitals. Additionally, the electron occupancy on the LP electron orbitals of nitrogen on both sides is symmetrical. After applying an electric field of 0.002 a.u., the interaction strength between the LP electron orbitals on the two nitrogen and the adjacent C-C antibonding orbitals becomes asymmetric, and the electron occupancy is no longer symmetrical. This observation is consistent with our dipole moment calculation results.

Subsequently, we calculated the NBO of the 2,6-NDA dimer, as shown in Figure S10b and Table S5. Our main concern was whether the nitrogen in the anchoring groups would influence the interaction strength between the two molecules after applying an electric field. However, the results indicate that the LP electron orbitals on the nitrogen do not exhibit stronger interactions with the other molecule as the electric field increases. Although the second-order perturbation energies between the LP electron orbitals on nitrogen and certain orbitals on the other molecule have increased, they remain at a very low level. Therefore, we attribute the observed increase in the LC peak of the 2,6-NDA molecular junction in the experiment primarily to the change in the molecular dipole moment with the applied electric field.

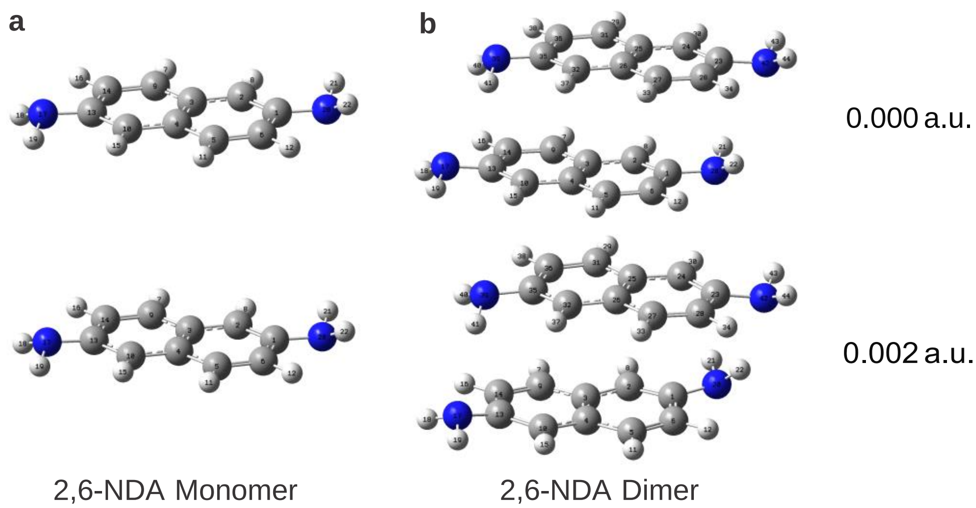

Figure S10. Natural bond orbital (NBO) analysis of the 2,6-NDA under zero and 0.002 a.u. electric field. (a) 2,6-NDA monomer. (b) 2,6-NDA dimer.

Table S4. NBO Analysis of the 2,6-NDA Monomer.

EF	Donor	Acceptor	$E^{(2)}$ kcal/mol	Occupancy
No field	LP N_{17}	RY* (3) C_{13} BD* (2) $C_{10} - C_{13}$	1.41 24.32	1.86480
	LP N_{20}	RY* (3) C_1 BD* (2) $C_1 - C_2$	1.41 24.32	1.86480
0.002 a.u.	LP N_{17}	RY* (3) C_{13} BD* (2) $C_{10} - C_{13}$	1.55 27.98	1.84652
	LP N_{20}	RY* (3) C_1 BD* (1) $C_1 - C_2$ BD* (2) $C_1 - C_2$	1.24 0.55 21.28	1.88070

NBO analysis of the 2,6-NDA monomer under zero and 0.002 a.u. electric field. The table lists the second-order perturbation energies between the lone pair (LP) electron orbitals on nitrogen (as donor) that interact with other orbitals (as acceptor), along with the electron occupancy of the LP electron orbitals.

Table S5. NBO Analysis of the 2,6-NDA Dimer.

EF	Interaction	Donor	Acceptor	$E^{(2)}$ kcal/mol	Occupancy
No field	Form unit 1 to unit 2	LP N_{17}	BD* (1) $N_{39}-H_{40}$ BD* (1) $N_{39}-H_{41}$	0.13 0.09	1.87000
		LP N_{20}	RY* (4) C_{23} RY* (6) C_{23} BD* (2) $C_{23}-C_{24}$	0.09 0.06 0.07	1.85729
	Form unit 2 to unit 1	LP N_{39}	RY* (4) C_{13} RY* (6) C_{13} BD* (2) $C_{10}-C_{13}$	0.09 0.06 0.07	1.85729
		LP N_{42}	BD* (1) $N_{20}-H_{21}$ BD* (1) $N_{20}-H_{22}$	0.09 0.13	1.87000
0.002 a.u.	Form unit 1 to unit 2	LP N_{17}	BD* (1) $N_{39}-H_{41}$	1.42	1.85813
		LP N_{20}	RY* (3) C_{24} RY* (4) C_{25}	0.16 0.07	1.87506
	Form unit 2 to unit 1	LP N_{39}	RY* (4) C_{13} RY* (7) C_{13} RY* (3) C_{14} BD* (2) $C_{9}-C_{14}$ BD* (2) $C_{10}-C_{13}$	0.07 0.05 0.07 0.28 0.10	1.83797
		LP N_{42}	RY* (1) H_{22} BD* (1) $N_{20}-H_{22}$	0.08 2.41	1.88050

References

1. Y. Chen, H.-C. Wang, Y. Tang, Y. Zhou, L. Huang, J. Cao, *et al.*, *Chem. Commun.*, 2021, **57**, 1935-1938.
2. K. Yoshizawa, T. Tada and A. Staykov, *J. Am. Chem. Soc.*, 2008, **130**, 9406-9413.
3. C. J. Lambert and S. X. Liu, *Chem. Eur. J*, 2018, **24**, 4193-4201.
4. P. Li, S. Hou, B. Alharbi, Q. Wu, Y. Chen, L. Zhou, *et al.*, *J. Am. Chem. Soc.*, 2022, **144**, 15689-15697.